Arch Biol Sci. 2023;75(2):141-154 https://doi.org/10.2298/ABS230220012V

Distribution of interstitial cells of Cajal and nerve fibers in rat stomach in streptozotocin-nicotinamide-induced diabetes mellitus

Aleksandra I. Veličkov[1,*], Vladimir Petrović[1], Branka Djordjević[2], Asen V. Veličkov[3], Aleksandar Petrović[1], Milica Lazarević[1] and Julija Cvetković[4]

[1]*University of Niš, Faculty of Medicine, Department of Histology and Embryology*, 18000 Niš, Serbia
[2]*University of Niš, Faculty of Medicine, Department of Biochemistry*, 18000 Niš, Serbia
[3]*University Clinical Center Niš, Clinic for Orthopedic Surgery and Traumatology*, 18000 Niš, Serbia
[4]*University Clinical Center Niš, Center for Pathology*, 18000 Niš, Serbia

***Corresponding author**: acka13v@gmail.com

Received: February 20, 2023; **Revised**: March 15, 2023; **Accepted**: March 17, 2023; **Published online**: March 31, 2023

Abstract: Diabetic peristalsis disorders are common complications in diabetes mellitus type 2. Disturbance of interstitial cells of Cajal (ICC) caused by metabolic changes in diabetes could explain the symptoms of diabetic gastroenteropathy. Although heterogenous interstitial cell types represent only 5% of the cell population of the muscle layer in the gastrointestinal tract (GIT), they are important for conducting electrical signals and regulating muscle excitability. The aim of this study was to investigate the alterations of the myenteric and intramuscular ICCs in the gaster of rats with diabetes mellitus type 2 (DMT2), as well as determine their distribution in relation to smooth muscle cells and enteric nerve structures. Male Wistar rats were used and DT2 was induced by streptozotocin-nicotinamide (STZ-NA) application. The stomach specimens were exposed to type III transmembrane tyrosine kinase (c-KIT), neurofilament (NF-M) protein and desmin antibodies to investigate the ICC, enteric neurons and smooth muscle cells. Morphological changes of the cells were quantified by the numerical areal density of intramuscular ICC, the ICC score of myenteric ICC and the volume density of nerve fibers. In conclusion, a statistically significant decrease in the number of intramuscular ICC and myenteric ICC without nerve fiber loss were observed in all stomach regions in rats with STZ-NA-induced DMT2.

Keywords: diabetes mellitus type 2; interstitial cells of Cajal; stomach (gaster); streptozotocin; nicotinamide

INTRODUCTION

The global incidence and prevalence of diabetes mellitus type 2 (DMT2) continues to rise across all regions of the world and is projected to increase to 7079 individuals per 100,000 by 2030 [1]. In addition to microvascular complications (nephropathy, retinopathy, peripheral polyneuropathy) and frequent infections, 50-70% of patients with DMT2 have some gastrointestinal motility disturbance such as dysphagia, gastroesophageal reflux, heartburn, abdominal discomfort or pain, gastralgia, gastroparesis, nausea and vomiting, slowed intestinal transit, constipation, diarrhea, fecal incontinence [2,3]. The average incidence of gastric dysmotility, such as gastroparesis, is about 9.4% in DMT2 patients [4]. Nutritional deficiencies with metabolic disorders are common in patients with gastroparesis and on occasion, a jejunal tube needs to be applied to bypass the stomach in severe cases [5].

Most studies that examine the mechanism of diabetic gastroenteropathy are based on the pathophysiology of peripheral or autonomic neuropathy. However, in addition to the enteric nerves, diabetes could cause changes in other regulatory factors of gastric peristalsis, such as smooth muscle cells, interstitial cells of Cajal (ICCs) and the endothelium of ganglion capillaries [6]. The identification of cellular biomarkers may help in developing better strategies for the diagnosis and management of patients with diabetic gastroenteropathy. Although ICC are sparingly distributed across the muscular layer of the gastrointestinal tract (GIT) and represent only 5% of the cell population in the

How to cite this article: Veličkov AI, Petrović V, Djordjević B, Veličkov AV, Petrović A, Lazarević M, Cvetković J. Distribution of interstitial cells of Cajal and nerve fibers in rat stomach in streptozotocin-nicotinamide-induced diabetes mellitus. Arch Biol Sci. 2023;75(2):141-54.

gastric wall, they are necessary for the establishment and adequate functioning of peristalsis [7].

ICC are morphologically and functionally "inserted" between the elements of the enteric nervous system and the smooth muscle cells of the GIT musculature from the esophagus to the internal anal sphincter. Although they were described more than a hundred years ago, the discovery in 1992 that these cells possess tyrosine-protein kinase KIT (c-KIT) activity has enabled their immunohistochemical identification. It was also shown that they do not represent primitive nerves as was believed until then, but that they are cells of mesenchymal origin [8]. In addition to identifying ICC using c-KIT immunohistochemistry, ultrastructural electron microscopy analysis has revealed that ICC exhibit a specific distribution, arrangement and distinct morphological features depending on their localization within the different layers of the GIT wall [9-11]. ICC are interconnected and arranged in the form of linear bundles or three-dimensional networks of cells, which are classified based on their morphology, location and function into several subtypes: submucosal (ICC-SM), myenteric plexus (ICC-MP), intramuscular (ICC-IM), deep muscular plexus (ICC-DMP), subserous and septal ICC [9,12]. In the stomach, the two major ICC types determining gastric motility are ICC-IM and ICC-MP [13]. ICC-MP are stellate, branched, multipolar cells that form a network around the ganglions of the myenteric plexus with a primary role in generating slow depolarization waves (as peristalsis pacemakers) and in regulating the progression and duration of the GIT musculature contraction [14,15].

ICC-IM are spindle-shaped, long, thin cells that can be classified by their localization into ICC-IM of the circular sublayer (ICC-IMc) and ICC-IM of the longitudinal muscle sublayer (ICC-IML). Some stomach and colon ICC-IM parts can be networked into long linear cell arrays [16]. ICC-IML are similar in shape to the ICC-IMc, but they are less numerous throughout the entire GIT [9]. The function of the ICC-IM is to mediate cholinergic and nitrergic neurotransmission [13,17] and act as a sensory transducer of mechanical stimuli during the feedback that affects motility. They also serve as stretch receptors [18]. ICC-IM participate in afferent signaling and integration of sensory-motor function as an element of the afferent branch of the gastrointestinal reflex [19].

ICC are very sensitive to changes in their microenvironment, especially to the absence of steel (stem cell) factor (SCF), the Kit receptor ligand, which is necessary for ICC differentiation, proliferation and survival [20]. Loss and dysfunction of ICC have been shown in numerous studies of GIT motility disorders [21-23].

Symptoms of diabetic gastroenteropathy are often overlooked and attributed to other causes and accompanying diseases. Various motility disorders associated with diabetes have been observed in the stomach. Diabetes mellitus (DM) is associated with rapid early gastric emptying, especially in the early stages of the disease [24], and as a complication of DM, delayed gastric emptying and gastroparesis are more often present [25,26]. The inadequate relaxation of the gastric fundus is responsible for early satiety and symptoms of dyspepsia [27]. Electrophysiological studies have shown slow-wave contraction dysrhythmias, prolonged pyloric contractions and impaired coordination between the antrum and duodenum [28,29]. To understand the onset mechanisms of the diabetic gastroenteropathy caused by DMT2, it is necessary to study the morphological changes of the GIT and changes in cell distribution in experimental animal models since the sampling of the entire thickness of the GIT wall in humans (patients and controls) is impractical because the muscle layer depth is not reached during routine biopsies. Several animal models of diabetes (primarily type 1 diabetes) have shown that changes and loss of ICC occur in the GIT [30-34]. In this paper, the focus was on morphological and numerical changes of distinct ICC types in an animal model of DMT2 (a type of diabetes found in 95% of diabetic patients) since there is neither accurate nor sufficient information in the literature about the distribution of ICC in different stomach parts in this animal model. The objective of the present study was to investigate alterations of the myenteric and intramuscular ICC in the gaster of rats in STZ-NA-induced DMT2, as well as to determine their distribution in relation to smooth muscle cells and enteric nerve structures.

MATERIALS AND METHODS

Ethics statement

The experimental protocol was approved by the Ethics Committee of the Faculty of Medicine, University of Niš, Serbia (permits No. 12-519/7 and 01-10204-3).

The study complied with the National Guide for the Care and Use of Laboratory Animals published by the Academy of Sciences and Rulebook for Handling Laboratory Animals of the Faculty of Medicine, University of Niš, Serbia. The protocol was performed at the Faculty of Medicine, University of Niš, at the Research Center for Biomedicine and the Department for Histology and Embryology.

Animals

The experiment was conducted on healthy 10-week-old male Wistar rats weighing 230-250 g. During the experiments, the rats were housed in plastic cages in the vivarium of the Research Center for Biomedicine, University of Niš, in a controlled environment of air humidity, ventilation and temperature (20°C±2°C). The rats were kept in a constant 12 h light/dark cycle with unrestricted access to food and water.

Experimental grouping

After acclimatization for one week, the animals were randomly divided into two groups as follows: (i) C group – control group; (ii) streptozotocin-nicotinamide induced diabetes – STZ-NA group (DMT2 animal model). This animal type 2 diabetes model was introduced and described by Masiello et al. [35].

Animal model

Diabetes mellitus type 2 was induced in the STZ-NA group by an intraperitoneal (i.p.) injection of freshly prepared streptozotocin (Sigma Aldrich, USA) at a dose of 45 mg/kg in an ice-cold, 0.1-mol/L citrate buffer (pH 4.5) following i.p. injection of nicotinamide (Sigma Aldrich, USA) at dose 110 mg/kg in saline solution after an overnight fast. The animals from the C group received an i.p. injection of citrate buffer and saline solution. Fasting and non-fasting glucose levels were determined in blood obtained from the tail vein on the 3rd and 7th days after STZ-NA administration using the glucose meter Accu-check Performa (Roche Diagnostics, USA) to confirm hyperglycemia. The animals with glucose levels >8.3 mmol/L were considered diabetic according to the criteria for diagnosing diabetes [36], while the rest of the animals were excluded from the experiment, so 12 animals entered the experiment per group (n=12). Serum insulin levels were measured with a commercial rat enzyme-linked immunosorbent assay (ELISA) kit using rat insulin as the standard (Mercodia, Upsala, Sweden; catalog number 10-1250-01). The body mass of the animals was continuously monitored, with measurements performed once a week, as well as on the day of sacrifice. The animals' food and water consumption were monitored daily. The animals were weighed on a scale after overnight fasting. Six weeks after the onset of DMT2, the animals were sacrificed by exsanguination after bilateral thoracotomy in deep anesthesia (ketamine hydrochloride, 100 mg/kg body weight). Before sacrifice, the glycemia of the animals was determined under the same conditions as at the beginning of the experiment, after 2 h and 8 h of fasting.

Tissue preparation

Immediately after exsanguination, the entire GIT was dissected in a block via an abdominal incision. The stomach was cut distally with the initial part of the duodenum, and then a longitudinal section was made along the great curve of the stomach. The initial part of the stomach (cardia and fundus), the central part of the corpus and the pylorus with the proximal portion of the duodenum were sampled separately, and their contents were washed with saline solution. All full-thickness samples were fixed in buffered formalin (10%) for 24 h and paraffin-embedded by the routine procedure. The 4-5μm-thick longitudinal tissue sections were cut on a Leica microtome, adhered on microscopic slides for immunohistochemistry (SuperFrost UltraPlus ground edges 90°, Thermo Scientific Menzel-Glazer), and stained as described below.

Hematoxylin and eosin (HE) staining method

The tissue slides were deparaffinized at 58°C with xylene and rehydrated in descending series of ethanol concentrations (100%, 96%, 70%) and distilled water. Hematoxylin was applied for 8 min and the dye was differentiated under the tap water, followed by rinsing in distilled water. Eosin was applied for 20 min, followed by rinsing in distilled water. The tissue slides were dehydrated in ascending series of alcohols (70%, 96%, 100%) and cleared in xylene. The coverslips were mounted using Canada balsam.

Immunohistochemistry

After the deparaffinization (at 58°C with xylene) and rehydration in descending series of ethanol concentrations (100%, 96%, 70%) and distilled water, the histological slides were submitted to an antigen retrieval procedure for 15 min, performed at 95-98°C in the antigen retrieval solution provided in the EnVision Flex visualization kit (DM 828, 50x, Dako, Denmark). After the three rinses in distilled water, the endogenous peroxidase was blocked using a 3% hydrogen solution for 10 min. The tissue samples were incubated overnight with primary antibody at 4°C. The primary antibodies used in the research were: rabbit monoclonal anti-c-KIT antibody (Abcam, Cambridge UK, Ab32363, dilution 1:100 with 24 h overnight incubation at 4°C) for ICC identification; rabbit polyclonal anti-Neurofilament M (NF-M) antibody (Abcam, Cambridge UK, Ab9034, dilution 1:100 with 24 h overnight incubation at 4°C) for nerve structures analysis; and Desmin Monoclonal Mouse anti-Human Clone D33 (Daco, Denmark, MO760, dilution 1:100 with 1.5 h incubation at room temperature) for smooth muscle cells analysis. Incubation with the secondary antibody was performed for 45 min (EnVision FLEX High pH, code number K8000, Dako, Denmark). The immune complexes were visualized by the Daco REAL EnVision Detection System (Dako, Denmark). The tissue slides were then counterstained with hematoxylin, dehydrated in ascending series of alcohols (70%, 96%, 100%) and cleared in xylene. The coverslips were mounted using Canada balsam.

Qualitative analysis of tissue samples

Description analysis of the tissue samples stained with HE, and immunohistochemically with c-KIT, NF-M and desmin antibodies was performed under a light microscope Olympus BX50 equipped with a Leica DFC 295 digital camera (Leica Micro-System, Rueil-Malmaison, France). Photomicrographs were taken under different magnifications in tif. format. On the slides stained with HE the general histological structure was observed and the absence of inflammation was confirmed. The pattern of distribution, localization and morphology of c-KIT Immunopositive cells, nerve fibers and smooth muscle cells were observed.

Quantitative image analysis

The following parameters were examined: numerical areal density (N_A) of ICC-IM and ICC-MP score in c-KIT immunolabeled slides, volume density (V_V) of nerve fibers in NF-M immunolabeled slides, and the thickness of muscle layer on desmin immunolabeled slides.

Numerical areal density represents the average number of cells per mm^2 of tissue. The images for analysis of N_A of ICC-IM were obtained on an Olympus BX50 light microscope equipped with a Leica DFC 295 digital camera (Leica Micro-System, Rueil-Malmaison, France). The photomicrographs were taken at the magnification ×200. N_A of ICC-IM was determined separately in circular and longitudinal muscle layers. For N_A of ICC-IM, we used the digital image analysis software ImageJ (National Institute of Health, Bethesda, MD, USA; http://imagej.nih.gov/ij/), and the following formula: $N_A = (10^6 xN)/A$, (N – number of the cells counted in muscle layer in the visual field, A – the area of the muscle layer in mm^2). The number of ICC-IM in both circular and longitudinal muscular layer on each slide was counted manually to avoid c-KIT-positive mast cells, which differ from ICC in shape, granular content and location. The number of examined visual fields per part of the stomach (cardia, corpus, pylorus) in the control and experimental groups is given in Table S4.

The ICC-MP network surrounding the myenteric plexus was evaluated by ICC-MP score, according to the recommendations of the International Working Group for Gastrointestinal Neuromuscular Diseases using the den Braber-Ymker [37] semiquantitative method. The ICC-MP score represents the percentage of myenteric ganglion encirclement by the processes of ICC-MP; the score is ranked from 0 to 100%, with a grade of 0% representing the absence of c-KIT-positive cells around the MP ganglion, while a grade of 100% represents ganglions completely surrounded by the body and processes of ICC-MP. Examination of the MP ganglions was performed under magnification ×400 on an Olympus BX50 light microscope equipped with a Leica DFC 295 digital camera (Leica Micro-System, Rueil-Malmaison, France). The whole muscular layer of the histological sections of each examined stomach part was observed for the presence of MP ganglions. The number of analyzed ganglions is presented in Table S5.

The distribution of nerve elements was analyzed by determining the volume density of NF-M-positive fibers in the muscle layer. Volume density (V_V) is a relative variable that shows how much the observed space in volume units occupies the overall space. The V_V was determined using the following formula: V_V = Vf/Vt. Vt is the total number of points of the grid overlaid by the photomicrograph, while Vf is the number of points overlapping the examined structure. The obtained results were multiplied by 100 and presented as percentages. We used the ImageJ software and grid plugin to insert the grid system with 336 points (area per point 3,957.66 μm2) to analyze the nerve fibers and ganglia volume density. The number of points overlapping the nerve fibers and ganglia (Vf) within the stomach muscle layer was counted.

The thickness of the muscle layer was determined using ImageJ software on the desmin immunohistochemical slides. For this analysis, 120 visual fields per group were examined per part of the stomach (cardia, corpus and pylorus), i.e., 10 visual fields per animal. The measurements were performed under magnification ×200. After the calibration of the image, the tree measurements were taken for the thickness of the muscle layer and the average value was taken as a thickness value for the examined visual field.

Statistical analysis

Statistical analysis was performed using SPSS Statistics (version 20, SPSS, Chicago, USA). The results were presented as mean±standard deviations (mean±SD). The obtained values were compared using the Kruskal-Wallis test followed by the Mann-Whitney U post hoc test since the coefficient of variation (CV) for the obtained values was >30.

RESULTS

Establishment of the DMT2 rat model

The STZ-NA model has already shown benefits in experimental studies and is widely used as a model of diabetes that corresponds to DMT2 in humans, characterized by mild non-fasting hyperglycemia and slightly decreased insulin levels [38], as reported in our recent study [39]. Animals in the diabetic group showed significantly higher final body weight (P<0.05) compared to the control group (Table 1). As shown in Table 1, blood glucose levels were significantly higher (P<0.001), followed by lower serum insulin levels (P<0.05) in the STZ-NA group compared to the control. In addition, in the STZ-NA group, moderate polydipsia and polyphagia were observed.

Table 1. Average body weight, glycemia, insulinemia, food and water consumption per animal in control and diabetic (STZ-NA) rats.

Parameters	Group	
	Control	STZ–NA
Initial body weight (g)	351.7±7.5	352.5±14.9
Final body weight (g)	395.0±12.3	413.7±19.2 **
Fasting blood glucose levels (mmol/L)	4.75±0.20	6.63±0.34 *
Non-fasting blood glucose levels (mmol/L)	6.36±0.01	12.02±1.65 *
Serum insulin levels (pmol/L)	217.1±21.2	191.2±16.3 **
Food consumption (g/day)	29.1±3.9	36.6±3.2*
Water consumption (mL/day)	40.2±5.1	56.3±6.5*

Values are expressed as the mean±SD of the mean; *statistical significance (P<0.001), **statistical significance (P<0.05).
The above data have already been reported in our recent study [39].

Histological and morphometric analysis

In the rat stomach-muscle wall of the STZ-NA group there were no signs of necrosis or apoptosis and no evidence of neutrophil or lymphocyte infiltration (Fig. 1A, B). Further, desmin immunoreactivity was present in the muscle layers of the rat stomach wall (Fig.1 C, D) in both experimental groups, and there was no difference in the muscle layer thickness between the groups (Table 2). In the corpus and pylorus regions, NF-M immunohistochemistry showed the presence of ganglion cells of the myenteric plexus (MP) on the longitudinal sections of the stomach of the control and STZ-NA groups (Fig. 1 E, F). No differences were found between groups in the distribution and morphology of MP ganglia and NF-M-positive nerve fibers. Analysis of volume density (V_V) of the NF-M-positive

Table 2. Thickness of stomach muscle layer in control and diabetic (STZ-NA) rats.

Muscle wall thickness (μm)			
Group	Cardia	Corpus	Pylorus
Control	369.015±29.57	355.152±28.41	406.152±26.23
STZ-NA	363.441±27.31	360.786±35.57	415.786±27.31

Values are expressed as the mean±SD of the mean.

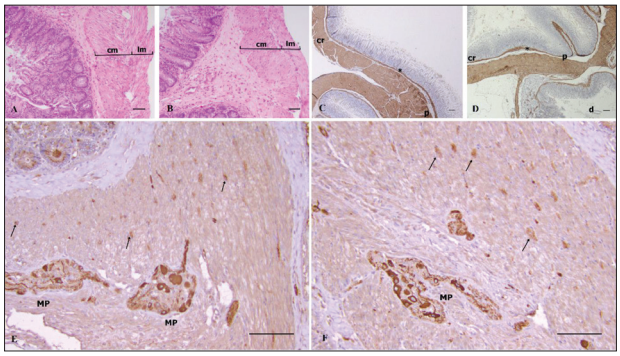

Fig. 1. H&E, desmin and NF-M immunohistochemistry of the rat stomach in control and diabetic group. **A** – stomach corpus of control group; H&E ×100, **B** – stomach corpus of STZ-NA group; H&E ×100, **C** – stomach corpus and pylorus of control group; desmin immunohistochemistry ×40, **D** – stomach corpus and pylorus of STZ-NA group; desmin immunohistochemistry ×40, **E** – pylorus of control group; NF-M immunohistochemistry ×200, **F** – pylorus of STZ-NA group NF-M immunohistochemistry ×200. In the wide circular (cm) and thin longitudinal (lm) muscle layer of control and diabetic group (A, B) there were no signs of lymphocyte infiltration, apoptosis or necrosis. Desmin immunoreactivity was present in thin lamina muscularis mucosae (asterisk) and muscle layer (m) of corpus (cr), pylorus (p) and duodenum (d) in control and diabetic group rat stomach (C, D). NF-M immunoreactive myenteric plexus ganglions (MP) and nerve fibers (arrow) in control and diabetic group (E, F). Bar = 100 μm.

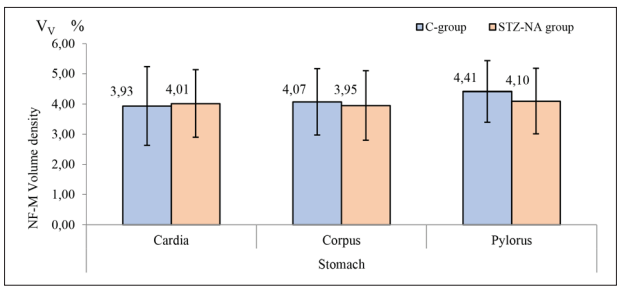

Fig. 2. Volume density of NF-M-positive fibers in the muscle layer of the rat stomach in control and STZ-NA group, 12 animals per group. There were no differences in the volume density of NF-M-positive nerve fibers between groups and between regions of cardia, corpus and pylorus. Numerical values presented in the figure correspond to the mean values of the NF-M volume density.

nerve fiber values in the examined stomach parts showed no statistically significant difference among the groups (Fig. 2).

In both experimental groups, immunoreactive c-KIT cells identifiable as ICC-IM were present in the muscle layer of different anatomical locations of rat stomach (cardia and fundus, corpus, pylorus). Intramuscular ICC were seen as spindle-shaped, bipolar cells with two long processes located within the

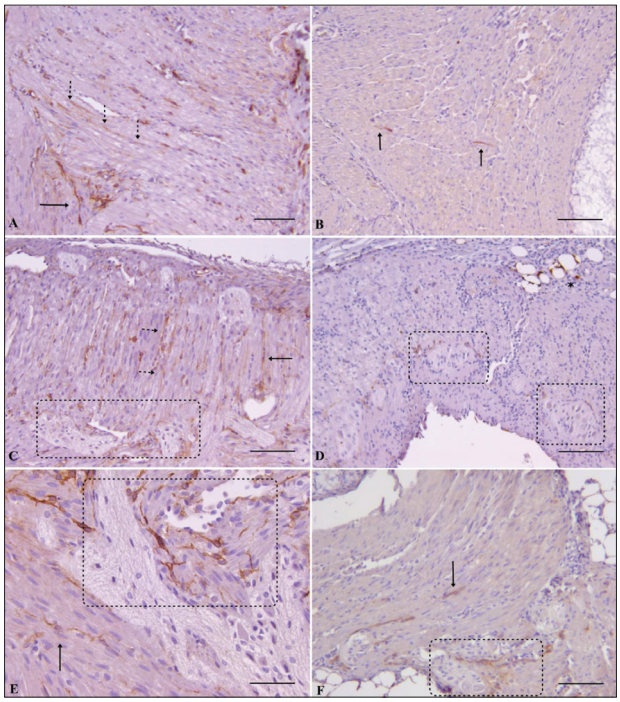

Fig. 3. C-kit immunohistochemistry of rat stomach in control and diabetic group. **A** – cardia of control group; ×200, **B** – cardia of STZ-NA group; ×200, **C** – stomach corpus of control group; ×200, **D** – stomach corpus of STZ-NA group; ×200, **E** – pylorus of control group; ×400, **F** – pylorus of STZ-NA group; ×200. Spindle-shaped ICC-IM (arrow) were densely distributed through the circular muscle layer of the cardia, corpus and pylorus of the control group rats (A, C, E). They had two long processes originating from their opposite poles (E) and most commonly they were single, but also merged into long linear arrays (dashed arrow). Spindle shaped ICC-IM of the STZ-NA were rare and mostly seen as single cells (B, D, F). Multipolar ICC-MP were densely distributed at the boarder of the circular and longitudinal muscle sublayer and around the myenteric plexus ganglion (dashed line) in the corpus and pylorus (C, E) in control group, while in STZ-NA group these cells scarcely surrounded ganglions. Oval mast cell seen in submucosa (asterisk). Bar A-D, F=100 μm, E=50 μm.

circular and longitudinal muscle layers in parallel to the longitudinal axis of the smooth muscle cells (Fig.3). The density of ICC-IM was significantly higher in the circular muscle layer compared to the density of ICC-IM of the longitudinal muscle sublayer in all anatomical regions of the stomach (Fig.4).

ICC-IM were densely distributed through the circular muscle layer of the cardia, fundus and part of the corpus, while multipolar c-KIT cells corresponding to ICC-MP were completely absent in the cardia regions. ICC-MP were present in the lower parts of the corpus, antrum and pylorus, while the number

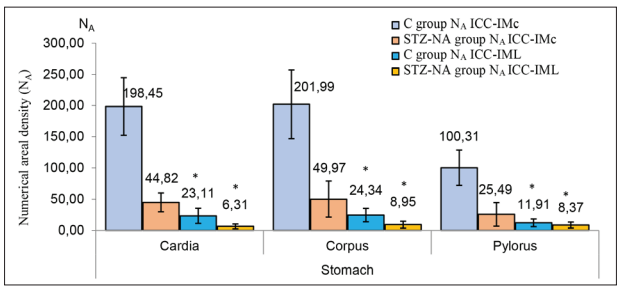

Fig. 4. Numerical areal density (N_A) of intramuscular ICC of the circular (ICC-IMc) and longitudinal (ICC-IML) muscle layer of the rat stomach in control and STZ-NA group, 12 animals per group. Numerical values presented in the figure correspond to the mean values of the N_A of ICC-IM, * – statistical significance (P<0.001).

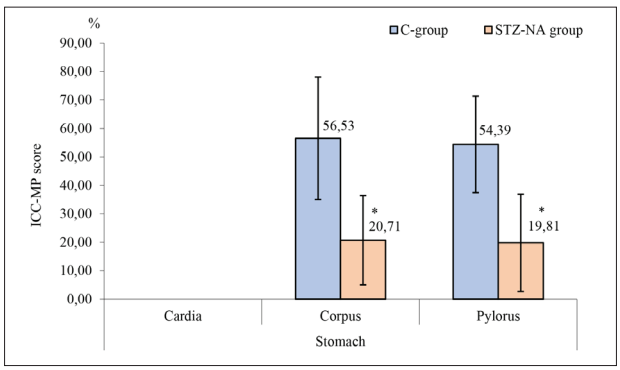

Fig. 5. Myenteric interstitial cells of Cajal (ICC-MP) score in the muscle layer of the rat stomach in control and STZ-NA group, 12 animals per group. Numerical values presented in the figure correspond to the mean values of the ICC-MP score, * – statistical significance (P<0.001).

of ICC-IM in these regions decreased. In the control group, ICC-IM, particularly in the cardia and pylorus regions, often merged into long linear arrays (Fig.3 A, C). ICC-IM networking into linear arrays was not observed anywhere in the longitudinal muscle layer of either experimental group. In the diabetic group, ICC-IM showed the same morphology except that their number was reduced. ICC-IM of the STZ-NA group were mostly seen as single cells or were completely absent from the visual field (Fig.3, B, D, F). There were statistically significant differences (P<0.001) in the numerical areal density (N_A) of ICC-IM values in examined parts of the stomach between the groups, indicating a significantly reduced number of these cells in the diabetic group (Fig.4).

ICC-MP were situated around the ganglion of the myenteric plexus between the circular and longitudinal muscle layers of the corpus and pylorus. They were multipolar, stellate cells with 3-5 primary cytoplasmic processes that branched secondarily and tertiarily and also interconnected with the processes of the nearby ICC-MP in a three-dimensional network around the ganglion without extending into the ganglion (Fig.3 E). In the control group, these cytoplasmatic processes surrounded the MP up to 80%, while in the diabetic group, these cells scarcely surrounded ganglions (approximately from 10% to 40%). The values of the ICC-MP score in the corpus and pylorus showed a statistically significant difference in the percentage encirclement of the ganglion by the processes of ICC-MP (P<0.001), possibly indicating a decrease in ICC-MP number or morphological changes with a reduction in cytoplasmatic processes in the diabetic group, as shown in (Fig. 5).

Immunoreactive c-KIT-positive mast cells were also found in addition to ICC in both groups. They could be distinguished from the ICC by size, shape, lack of processes, granular content and location. Their localization appeared predominantly in the mucosa between glands, in the submucosa and scattered through the connective tissue septa in the muscle layers.

DISCUSSION

In the STZ-NA rat model, glucose tolerance disorder was induced by applying two components: streptozotocin (STZ), a well-known diabetogenic agent with cytotoxic activity on pancreatic beta cells, and nicotinamide (NA), which is a neuron and beta-cell protector. The STZ-NA model has already shown benefits in experimental studies and is widely used as a model of diabetes that corresponds to DMT2 in humans, characterized by mild non-fasting hyperglycemia and slightly decreased insulin levels [38], as reported in our recent study [39]. Animals in this model do not require exogenous insulin administration to survive. Hyperglycemia is identified as a risk factor for the development of diabetic gastroenteropathy [40]. In this experiment, only male rats were used, as proposed by Masiello [35]. It was shown that female diabetic rats manifested lower glycemia levels than diabetic males and that estrogen enhances insulin sensitivity and protects against oxidative stress in diabetic females [41].

There are no data on ICC distribution in the stomach in the STZ-NA model in the literature. Our recent study showed a decrease in the number of intramuscular ICC and myenteric ICC in the caecum, proximal and distal colon in rats with type 2 diabetes [39]. Unlike other diabetes models from the literature in which the ICC distribution was observed [13,32], STZ-NA rats do not develop neuropathy, myopathy or smooth muscle cell atrophy as complications of diabetes mellitus [42-43]. Smooth muscle cells with nerves and ICC form a functional syncytium necessary to maintain the normal contractile function of the GIT. Diabetes causes numerous complications in the GIT, with consequent changes in all cellular elements of this physiological syncytium, and the pathogenetic mechanism of diabetic gastroenteropathy is also complex. With the STZ-NA model, it is possible to control the diabetogenic damage to nerve structures and smooth muscle cells in diabetes, which enables the examination of ICC independently of the cause-and-effect relationships of the other cells of the syncytium.

In the STZ-NA group, no atrophy of smooth muscle cells was observed, nor was there any difference in the thickness of the muscle wall compared to the control group. Also, there were no signs of necrosis, apoptosis or inflammation in any of the stomach samples of the STZ-NA group. The results of the nerve fibers Vv showed that there were no differences in the density of nerve fibers, i.e., that neuropathy did not develop in rats as a complication of diabetes, which contrasts with previous studies of ICC in diabetes [32,44,45] where changes in GIT nerves were noted.

In this study, ICC-IM merged into long linear arrays in the circular muscle layers of the cardia and pylorus in the control group. Networking of ICC in these segments of the GIT is essential for the function of the gastric sphincter (lower esophageal sphincter, cardia and pylorus). The density of ICC-IM of the control group is significantly higher in the cardia and corpus compared to the pylorus, which can be explained by the fact that in the cardia, ICC-IM have the primary function in neurotransmission and support of relaxation of the lower esophageal sphincter [46]. Regional differences in the distribution of ICC-IM and ICC-MP in the stomach (ICC-MP appear in the lower parts of the corpus, antrum and pylorus and are not absent in the cardia, while ICC-IM are abundant in the cardia, and the number of ICC-IM decreases toward pyloric region) correspond to the described distribution of ICC in the literature [9]. Kito [13] reported that ICC-IM in the guinea pig corpus, which has no ICC-MP, adopt the role of slow-wave pacemakers. Gastric musculature activation is thought to originate from ICC-IM, which generate high-frequency slow waves in the corpus and determine the dominant frequency of waves in the stomach. ICC-IM slow waves activate the ICC-MP network, from where slow waves propagate downward, through the stomach's muscle bundles, causing depolarization and initiation of muscle contraction. The depolarization wave also initiates the ICC-IM response as a regenerative potential in wave propagation [47].

ICC-IM in the STZ-NA group were rare and did not establish a linear network as seen in the cardia and pylorus of the control group. Considering the role of ICC-IM, loss of ICC-IM in the circular muscle layer of the cardia and pylorus is thought to be related to increased basal tone and spontaneous activity of the lower esophageal sphincter and pyloric sphincter, which contributes to the symptomatology of diabetic gastroenteropathy [48,49].

ICC-MP were also present in the STZ-NA group but much less compared to the control group. Also, MP ganglions with only one or no ICC-MP were observed. ICC-MP score values in the STZ-NA group indicated a decrease in ICC-MP cytoplasmatic processes or a reduction in ICC-MP number. In addition, an ICC-MP score of less than 30% is considered pathological [37]. ICC-MP contribute to GIT transit as dominant pacemaker cells generating rhythmic depolarization, and a substantial loss of ICC-MP is a common feature of delays in gaster transit caused by spontaneous peristaltic dysfunction [50].

In their research on diabetic NOD mice, Ordog et al. [30] showed that the loss of ICC density begins in the corpus of the stomach and increases towards the antrum, affecting mainly ICC-MP. Although slow waves still occurred in these areas, they were abnormal in amplitude and frequency and did not propagate through the entire muscular layer of the stomach. There was no loss of ICC-IM in the fundus, but there was a large gap between the ICC and nerve fibers. On the other hand, in 25 patients with DM and gastric cancer who underwent gastrectomy, the study of gastric tissue did not show a decrease in ICC-MP, but only a decrease in the number of ICC-IM in the inner circular muscle

layer [51]. Contrary to these data, the results of this study show a diffuse loss of ICC, affecting all parts of the stomach equally, and involving both ICC-IM and ICC-MP equally.

Wang et al. [32] also noted ICC loss in the fundus and corpus of the stomach of rats with streptozotocin (STZ)-induced diabetes, particularly a decrease in ICC-IM density in the circular and longitudinal muscle layers with loss of the nerve fibers. They demonstrated in the STZ rat stomach a decreased density of ICC and structural degeneration in ICC-IM and associated nerves with a special emphasis on loss of synaptic connections, accompanied by a simultaneous reduction in nerve tissue. However, our study showed no nerve loss or morphological changes in smooth muscle cells. Unlike our study, in the study by Wang et al., only cytotoxic streptozotocin was applied in a higher dose without modulation by the protective effect of nicotinamide to establish DMT2 model. Moreover, the animals were treated for a longer period, and the hyperglycemia values (followed by oxidative stress) were significantly higher. We assume that in our study changes in nerve fibers did not occur due to the shorter duration of the experiment, lower hyperglycemia and the protective effect of nicotinamide. We believe we gave the experiment enough time to catch ICC changes before nerve fiber loss occurs. Therefore, we suggest that during the development of diabetic gastroenteropathy, the loss of ICC occurs first, followed by a reduction in nerve fibers.

Insulin and insulin-like growth factor-1 (IGF-1) play a significant role in the survival of ICC. Although these cells do not have a receptor for insulin or IGF-1, a signaling pathway via the SCF receptor is necessary for their survival and function. On the other hand, SCF is produced by smooth muscle cells and enteric neurons that have receptors for insulin and IGF-I and indirectly mediate the action of insulin and IGF-I on ICC [30,52]. SCF secretion in response to insulin and IGF-1 is believed to be necessary for the survival and functioning of ICC [53]. In this study, it is possible that the loss of ICC, without an observed loss of nerve fibers, was due to impaired intracellular SCF signaling and the sensitivity of ICC to reduced insulin levels in this STZ-NA model.

The importance of ICC function is becoming increasingly apparent in diabetic gastrointestinal dysmotility, and autonomic neuropathy is no longer considered the sole cause of diabetic gastroenteropathy. DMT2 significantly alters the microenvironment of ICC, leading to reduced survival of these cells. The mechanism of ICC disorders in diabetes is multifactorial, and the interaction between these factors is complex. Changes in ICC in diabetes can potentially result from hyperglycemia and associated oxidative stress, decreased insulin and IGF-1 signaling, autoimmune response, or their combinations due to an imbalance between factors that damage and factors that regenerate and maintain ICC [44,54]. Horvath et al. [52] showed that hyperglycemia with oxidative stress alone is not sufficient to affect ICC and their changes but that the reduction of IGF-I and insulin signaling in diabetes play a major role in ICC loss. In our recent study [55], loss of ICC was shown in moderate hyperglycemia, while treatment with antioxidants, which normalized hyperglycemia, had no effect on improving ICC loss, suggesting that hyperglycemia is not the main cause of changes and loss of ICC.

ICC have a key role in the normal functioning of the GIT (pacemaker function, neuromodulation and adequate function of the sphincters of the cardia and pylorus). ICC are a potential morphological marker in diabetes motility disorders, and both ICC number and morphology have been shown to be important in gastric electrophysiology [22]. The alterations of ICC observed in several human GIT disorders [56,57] can occur primarily as part of the pathological process itself, but they can also occur secondarily as damage caused by various mechanisms during the evolution of the pathological process, which is difficult to determine at the current level of research [58]. Regardless of the cause, a loss of ICC or the disruption of their network lead to motility dysfunction and possibly sensory disturbances, contributing to the disease's clinical picture. These findings emphasize the importance of ICC and point out that changes in ICC that occur in diabetes are one of the main factors in the development of diabetic gastroenteropathy.

Treatment of diabetic gastroenteropathy is usually challenging and often suboptimal and is based on alleviating symptoms, correcting nutritional abnormalities and targeting the underlying causes, enhancing gastric emptying, surgery and gastric electrical stimulation [59,60]. Therefore, ICC can be a target and a significant link in developing more effective therapies for diabetic gastroenteropathy.

CONCLUSIONS

A statistically significant decrease in the number of intramuscular ICC and myenteric ICC was observed in all stomach regions in rats with type 2 diabetes. There was no nerve fiber loss in the stomach-muscle wall of rats with STZ-NA-induced DMT2, and nerve fiber distribution and volume density did not show differences between the control and diabetic group. The animal model of STZ-NA-induced diabetes can be used in the study of ICC in conditions without the development of neuropathy and myopathy as complications in diabetes. Bearing in mind the essential function of ICC in GIT peristalsis, a loss of ICC-IM and ICC-MP might play a role in the pathogenesis of diabetic gastroenteropathy. This could be a promising target in the development of more effective therapies for diabetic motility disorders.

Funding: The study was supported through the Internal Scientific Research Project INT-MFN, No. 38/20, of the Faculty of Medicine, University of Niš.

Author contributions: Conceptualization, AIV and BD; methodology AIV, BD, and VP, software AVV and VP; validation, AIV, AVV, VP and AP; investigation AIV and BD, writing – original draft preparation AIV; writing – review and editing, VP and AVV; interpreting data, AIV, BD, ML and AVV, visualization, AIV and JC; supervision, VP. All authors have read and agreed to the published version of the manuscript.

Conflict of interest disclosure: The authors declare no conflict of interest.

Data availability: Data underlying the reported findings have been provided as part of the submitted article in the Supplementary Material.

REFERENCES

1. Khan MAB, Hashim MJ, King JK, Govender RD, Mustafa H, Al Kaabi J. Epidemiology of Type 2 Diabetes - Global Burden of Disease and Forecasted Trends. J Epidemiol Glob Health. 2020;10(1):107-11. https://doi.org/10.2991/jegh.k.191028.001
2. Fujishiro M, Kushiyama A, Yamazaki H, Kaneko S, Koketsu Y, Yamamotoya T, Kikuchi T, Sakoda H, Suzuki R, Kadowaki T. Gastrointestinal symptom prevalence depends on disease duration and gastrointestinal region in type 2 diabetes mellitus. World J Gastroenterol. 2017;23(36):6694-704. https://doi.org/10.3748/wjg.v23.i36.6694
3. Vinik AI, Maser RE, Mitchell BD, Freeman R. Diabetic autonomic neuropathy. Diabetes Care. 2003;26(5):1553-79. https://doi.org/10.2337/diacare.26.5.1553
4. Kaplan LM, McCallum RW, Koch KL, Sederman R HB. High prevalence and underdiagnosis of gastroparesis symptoms among patients with type 1 and type 2 diabetes mellitus. Gastroenterology. 2013;144(5):S107. https://doi.org/10.1016/S0016-5085(13)60393-5
5. Abdelsayed N, Juarez A, Carter M. Severe Gastroparesis Leading to Hypoglycemia and Subsequent Seizures. Cureus. 2022;14(10):e30527. https://doi.org/10.7759/cureus.30527
6. Kashyap P, Farrugia G. Diabetic gastroparesis: what we have learned and had to unlearn in the past 5 years. Gut. 2010;59(12):1716-26. https://doi.org/10.1136/gut.2009.199703
7. Sanders KM, Ward SM, Koh SD. Interstitial cells: regulators of smooth muscle function. Physiol Rev. 2014;94(3):859-907. https://doi.org/10.1152/physrev.00037.2013
8. Maeda H, Yamagata A, Nishikawa S, Yoshinaga K, Kobayashi S, Nishi K, Nishikawa S. Requirement of c-kit for development of intestinal pacemaker system. Development. 1992;116(2):369-75. https://doi.org/10.1242/dev.116.2.369
9. Komuro T. Structure and organization of interstitial cells of Cajal in the gastrointestinal tract. J Physiol. 2006;576(3):653-8. https://doi.org/10.1113/jphysiol.2006.116624
10. Komuro T. Atlas of Interstitial Cells of Cajal in the Gastrointestinal Tract. Springer;2012.134 p. https://doi.org/10.1007/978-94-007-2917-9
11. Faussone-Pellegrini M-S, Cortesini C, Romagnoli P. The ultrastructure of the muscle coat of human gastro-oesophageal junction, with special reference to "interstitial cells of Cajal". Front Neurosci. 2013;7:49. https://doi.org/10.3389/fnins.2013.00049
12. Al-Shboul OA. The importance of interstitial cells of Cajal in the gastrointestinal tract. Saudi J Gastroenterol. 2013;19(1):3-15. https://doi.org/10.4103/1319-3767.105909
13. Kito Y. The functional role of intramuscular interstitial cells of Cajal in the stomach. J Smooth Muscle Res. 2011;47(2):47-53. https://doi.org/10.1540/jsmr.47.47
14. Hwang SJ, Blair PJ, Britton FC, O'Driscoll KE, Hennig G, Bayguinov YR, Rock JR, Harfe BD, Sanders KM, Ward SM. Expression of anoctamin 1/TMEM16A by interstitial cells of Cajal is fundamental for slow wave activity in gastrointestinal muscles. J Physiol. 2009;587(20):4887-904. https://doi.org/10.1113/jphysiol.2009.176198
15. Huizinga JD, Zarate N, Farrugia G. Physiology, injury, and recovery of interstitial cells of Cajal: basic and clinical science. Gastroenterology. 2009;137(5):1548-56. https://doi.org/10.1053/j.gastro.2009.09.023
16. Ibba Manneschi L, Pacini S, Corsani L, Bechi P, Faussone-Pellegrini MS. Interstitital cells of Cajal in the human stomach: distribution and relationship with enteric innervation. Histol Histopathol. 2004;19(4):1153-64.
17. Ward SM, McLaren GJ, Sanders KM. Interstitial cells of Cajal in the deep muscular plexus mediate enteric motor neurotransmission in the mouse small intestine. J Physiol. 2006;573(1):147-59. https://doi.org/10.1113/jphysiol.2006.105189
18. Powley TL, Wang XY, Fox EA, Phillips RJ, Liu LWC, Huizinga JD. Ultrastructural evidence for communication between intramuscular vagal mechanoreceptors and inter-

stitial cells of Cajal in the rat fundus. Neurogastroenterol Motil. 2008;20(1):69-79.
19. Huizinga JD, Reed DE, Berezin I, Wang X-Y, Valdez DT, Liu LWC, Diamant NE. Survival dependency of intramuscular ICC on vagal afferent nerves in the cat esophagus. Am J Physiol Regul Integr Comp Physiol. 2008;294(2):R302-10. https://doi.org/10.1152/ajpregu.00398.2007
20. Beckett EAH, Ro S, Bayguinov YR, Sanders KM, Ward SM. Kit signaling is essential for development and maintenance of interstitial cells of Cajal and electrical rhythmicity in the embryonic gastrointestinal tract. Dev Dyn. 2007;236. https://doi.org/10.1002/dvdy.20929
21. Vanderwinden JM, Rumessen JJ. Interstitial cells of Cajal in human gut and gastrointestinal disease. Microsc Res Tech. 1999;47(5):344-60. https://doi.org/10.1002/(SICI)1097-0029(19991201)47:5<344::AID-JEMT6>3.0.CO;2-1
22. Mostafa RM, Moustafa YM, Hamdy H. Interstitial cells of Cajal, the Maestro in health and disease. World J Gastroenterol. 2010;16(26):3239. https://doi.org/10.3748/wjg.v16.i26.3239
23. Huizinga JD, Hussain A, Chen J-H. Interstitial cells of Cajal and human colon motility in health and disease. Am J Physiol Gastrointest Liver Physiol. 2021;321(5):G552-75. https://doi.org/10.1152/ajpgi.00264.2021
24. Choi KM, Zhu J, Stoltz GJ, Vernino S, Camilleri M, Szurszewski JH, Gibbons SJ, Farrugia G. Determination of gastric emptying in nonobese diabetic mice. Am J Physiol Liver Physiol. 2007;293(5):G1039-45. https://doi.org/10.1152/ajpgi.00317.2007
25. Intagliata N, Koch KL. Gastroparesis in type 2 diabetes mellitus: prevalence, etiology, diagnosis, and treatment. Curr Gastroenterol Rep. 2007;9(4):270-9. https://doi.org/10.1007/s11894-007-0030-3
26. Huang I-H, Schol J, Khatun R, Carbone F, Van den Houte K, Colomier E, Balsiger LM, Törnblom H, Vanuytsel T, Sundelin E, Simrén M, Palsson OS, Bangdiwala SI, Sperber AD, Tack J. Worldwide prevalence and burden of gastroparesis-like symptoms as defined by the United European Gastroenterology (UEG) and European Society for Neurogastroenterology and Motility (ESNM) consensus on gastroparesis. United Eur Gastroenterol J. 2022;10(8):888-97. https://doi.org/10.1002/ueg2.12289
27. Undeland KA, Hausken T, Aanderud S, Berstad A. Lower postprandial gastric volume response in diabetic patients with vagal neuropathy. Neurogastroenterol Motil. 1997;9(1):19-24. https://doi.org/10.1046/j.1365-2982.1997.d01-3.x
28. Hasler WL, Soudah HC, Dulai G, Owyang C. Mediation of hyperglycemia-evoked gastric slow-wave dysrhythmias by endogenous prostaglandins. Gastroenterology. 1995;108(3):727-36. https://doi.org/10.1016/0016-5085(95)90445-X
29. Chen JD, Lin Z, Pan J, McCallum RW. Abnormal gastric myoelectrical activity and delayed gastric emptying in patients with symptoms suggestive of gastroparesis. Dig Dis Sci. 1996;41(8):1538-45. https://doi.org/10.1007/BF02087897
30. Ordög T, Takayama I, Cheung WK, Ward SM, Sanders KM. Remodeling of networks of interstitial cells of Cajal in a murine model of diabetic gastroparesis. Diabetes. 2000;49(10):1731-9. https://doi.org/10.2337/diabetes.49.10.1731
31. Wu Y-S, Lu H-L, Huang X, Liu D-H, Meng X-M, Guo X, Kim YC, Xu WX. Diabetes-induced loss of gastric ICC accompanied by up-regulation of natriuretic peptide signaling pathways in STZ-induced diabetic mice. Peptides. 2013;40:104-11. https://doi.org/10.1016/j.peptides.2012.12.024
32. Wang X-Y, Huizinga JD, Diamond J, Liu LWC. Loss of intramuscular and submuscular interstitial cells of Cajal and associated enteric nerves is related to decreased gastric emptying in streptozotocin-induced diabetes. Neurogastroenterol Motil. 2009;21(10):1095-e92. https://doi.org/10.1111/j.1365-2982.2009.01336.x
33. Wang Q, Zang J, Huang X, Lu H, Xu W, Chen J. Colonic Dysmotility in Murine Partial Colonic Obstruction Due to Functional Changes in Interstitial Cells. J Neurogastroenterol Motil. 2019;25(4):589-601. https://doi.org/10.5056/jnm19136
34. Wang H, Zhao K, Shi N, Niu Q, Liu C, Chen Y. Electroacupuncture Regularizes Gastric Contraction and Reduces Apoptosis of Interstitial Cells of Cajal in Diabetic Rats. Front Physiol. 2021;12:560738. https://doi.org/10.3389/fphys.2021.560738
35. Masiello P, Broca C, Gross R, Roye M, Manteghetti M, Hillaire-Buys D, Novelli M, Ribes G. Experimental NIDDM: development of a new model in adult rats administered streptozotocin and nicotinamide. Diabetes. 1998;47(2):224-9. https://doi.org/10.2337/diab.47.2.224
36. Genuth S, Alberti KGMM, Bennett P, Buse J, Defronzo R, Kahn R, Kitzmiller J, Knowler WC, Lebovitz H, Lernmark A, Nathan D, Palmer J, Rizza R, Saudek C, Shaw J, Steffes M, Stern M, Tuomilehto J, Zimmet P. Follow-up report on the diagnosis of diabetes mellitus. Diabetes Care. 2003;26(11):3160-7. https://doi.org/10.2337/diacare.26.11.3160
37. den Braber-Ymker M, Heijker S, Lammens M, Nagtegaal ID. Practical and reproducible estimation of myenteric interstitial cells of Cajal in the bowel for diagnostic purposes. Neurogastroenterol Motil. 2016;28(8):1261-7. https://doi.org/10.1111/nmo.12831
38. Szkudelski T. Streptozotocin-nicotinamide-induced diabetes in the rat. Characteristics of the experimental model. Exp Biol Med. 2012;237(5):481-90. https://doi.org/10.1258/ebm.2012.011372
39. Veličkov AI, Djordjević B, Lazarević M, Veličkov AV, Petrović V, Jović M, Denčić T, Radenković G. Distributions of Platelet-Derived Growth Factor Receptor-α Positive Cells and Interstitial Cells of Cajal in the Colon of Rats with Diabetes Mellitus Type 2. Medicina. 2023;59(2):308. https://doi.org/10.3390/medicina59020308
40. Aronson D. Hyperglycemia and the pathobiology of diabetic complications. Adv Cardiol. 2008;45:1-16. https://doi.org/10.1159/000115118
41. Díaz A, López-Grueso R, Gambini J, Monleón D, Mas-Bargues C, Abdelaziz KM, Viña J, Borrás C. Sex Differ-

ences in Age-Associated Type 2 Diabetes in Rats-Role of Estrogens and Oxidative Stress. Oxid Med Cell Longev. 2019;2019:6734836. https://doi.org/10.1155/2019/6734836
42. He W-Q, Peng Y-J, Zhang W-C, Lv N, Tang J, Chen C, Zhang CH, Gao S, Chen HQ, Zhi G, Feil R, Kamm KE, Stull JT, Gao X, Zhu MS. Myosin light chain kinase is central to smooth muscle contraction and required for gastrointestinal motility in mice. Gastroenterology. 2008;135(2):610-20. https://doi.org/10.1053/j.gastro.2008.05.032
43. Touw K, Chakraborty S, Zhang W, Obukhov AG, Tune JD, Gunst SJ, Herring BP. Altered calcium signaling in colonic smooth muscle of type 1 diabetic mice. Am J Physiol Gastrointest Liver Physiol. 2012;302(1):G66-76. https://doi.org/10.1152/ajpgi.00183.2011
44. Ordög T, Hayashi Y, Gibbons SJ. Cellular pathogenesis of diabetic gastroenteropathy. Minerva Gastroenterol Dietol. 2009;55(3):315-43.
45. Yarandi SS, Srinivasan S. Diabetic gastrointestinal motility disorders and the role of enteric nervous system: current status and future directions. Neurogastroenterol Motil. 2014;26(5):611-24. https://doi.org/10.1111/nmo.12330
46. Dixit D, Zarate N, Liu LWC, Boreham DR, Huizinga JD. Interstitial cells of Cajal and adaptive relaxation in the mouse stomach. Am J Physiol Gastrointest Liver Physiol. 2006;291(6):G1129-36. https://doi.org/10.1152/ajpgi.00518.2005
47. Hirst GDS, Edwards FR. Electrical events underlying organized myogenic contractions of the guinea pig stomach. J Physiol. 2006;576(3):659-65. https://doi.org/10.1113/jphysiol.2006.116491
48. Farré R, Wang X-Y, Vidal E, Domènech A, Pumarola M, Clave P, Huizinga JD, Jiménez M. Interstitial cells of Cajal and neuromuscular transmission in the rat lower oesophageal sphincter. Neurogastroenterol Motil. 2007;19(6):484-96. https://doi.org/10.1111/j.1365-2982.2007.00901.x
49. Sanders KM, Ward SM, Friebe A. CrossTalk proposal: Interstitial cells are involved and physiologically important in neuromuscular transmission in the gut. J Physiol. 2016;594(6):1507-9. https://doi.org/10.1113/JP271600
50. Sanders KM. Spontaneous Electrical Activity and Rhythmicity in Gastrointestinal Smooth Muscles. Adv Exp Med Biol. 2019;1124:3-46. https://doi.org/10.1007/978-981-13-5895-1_1
51. Iwasaki H, Kajimura M, Osawa S, Kanaoka S, Furuta T, Ikuma M, Hishida A. A deficiency of gastric interstitial cells of Cajal accompanied by decreased expression of neuronal nitric oxide synthase and substance P in patients with type 2 diabetes mellitus. J Gastroenterol. 2006;41(11):1076-87. https://doi.org/10.1007/s00535-006-1909-8
52. Horváth VJ, Vittal H, Ordög T. Reduced insulin and IGF-I signaling, not hyperglycemia, underlies the diabetes-associated depletion of interstitial cells of Cajal in the murine stomach. Diabetes. 2005;54(5):1528-33. https://doi.org/10.2337/diabetes.54.5.1528
53. Lin L, Xu LM, Zhang W, Ge YB, Tang YR, Zhang HJ, Li XL, Chen JD. Roles of stem cell factor on the depletion of interstitial cells of Cajal in the colon of diabetic mice. Am J Physiol Gastrointest Liver Physiol. 2010;298(2):G241-7. https://doi.org/10.1152/ajpgi.90706.2008
54. Huizinga JD, Lammers WJEP. Gut peristalsis is governed by a multitude of cooperating mechanisms. Am J Physiol Gastrointest Liver Physiol. 2009;296(1):G1-8. https://doi.org/10.1152/ajpgi.90380.2008
55. Velickov A, Mitrovic O, Djordjevic B, Sokolovic D, Zivkovic V, Velickov A, Pantovic V, Urlih NP, Radenkovic G. The effect of bilberries on diabetes-related alterations of interstitial cells of Cajal in the lower oesophageal sphincter in rats. Histol Histopathol. 2017;32(6):639-47. https://doi.org/10.26226/morressier.596dfd5ad462b802923876c1
56. Vanderwinden JM, Rumessen JJ. Interstitial cells of Cajal in human gut and gastrointestinal disease. Microsc Res Tech. 1999;47(5):344-60. https://doi.org/10.1002/(SICI)1097-0029(19991201)47:5<344::AID-JEMT6>3.0.CO;2-1
57. Jain D, Moussa K, Tandon M, Culpepper-Morgan J, Proctor DD. Role of interstitial cells of Cajal in motility disorders of the bowel. Am J Gastroenterol. 2003;98(3):618-24. https://doi.org/10.1111/j.1572-0241.2003.07295.x
58. Farrugia G. Interstitial cells of Cajal in health and disease. Neurogastroenterol Motil. 2008;20(1):54-63. https://doi.org/10.1111/j.1365-2982.2008.01109.x
59. Singh R, Zogg H, Ghoshal UC, Ro S. Current Treatment Options and Therapeutic Insights for Gastrointestinal Dysmotility and Functional Gastrointestinal Disorders. Front Pharmacol.2022;13:808195. https://doi.org/10.3389/fphar.2022.808195
60. Quigley EMM. Drug Treatments for Gastroparesis-Why Is the Cupboard So Bare? Gastroenterology. 2023;164(4):522-4. https://doi.org/10.1053/j.gastro.2023.01.029

SUPPLEMENTARY MATERIAL

Raw Table S1. Fasting blood glucose levels, non-fasting blood glucose levels, serum insulin levels, initial body weight, final body weight, body weight, food and water consumption of rat in control and diabetic (STZ–NA) rats.

Group	Animal No	Glycemia (mmol/L)		serum insulin (pmol/L)	body weight (g)		consumption	
		fasting	non-fasting		initial	final	food (g/day)	water (mL/day)
Control group	1	4.58	6.36	216.95	343.4	393	27.3	29.9
	2	4.58	6.38	240.05	355.9	397.4	32.6	42.7
	3	4.58	6.36	236.06	355.3	371.4	34.8	35.9
	4	4.58	6.35	170.59	355.1	401.3	32	40.5
	5	4.58	6.35	218.63	354.7	381.6	33.2	45
	6	4.58	6.35	206.23	355.2	389	26.7	49.1
	7	4.58	6.35	227.13	344.4	383.1	21.9	43.9
	8	4.58	6.37	218.95	357.9	410.8	27.6	35.3
	9	4.58	6.35	231.67	342.2	408.1	31.7	39.1
	10	4.58	6.36	235.95	363.3	411	25.7	43.4
	11	4.58	6.37	183.96	338.9	399.5	25.4	38.8
	12	4.58	6.35	219.04	354.1	393.9	30.3	38.7
STZ-NA	1	7.43	13.16	195.15	369.1	406.2	36	62.2
	2	6.46	7.94	188.99	355.4	411.4	40.1	52.3
	3	6.46	12.45	166.33	342.4	421.1	38	64.4
	4	6.73	12	167.24	353	409.9	32.6	59.2
	5	6.77	12.9	182.87	364.8	371.5	35	63.1
	6	6.08	14.08	204.31	355.9	441.5	33.7	51.8
	7	6.75	12.87	185.44	343.2	425.3	33.5	49.4
	8	6.35	13.28	197.57	322.1	399.2	37.3	54.3
	9	6.88	10.48	195.9	367	402.2	32.5	45
	10	6.76	12.75	218.69	332	413.8	41.7	51.1
	11	6.49	10.91	212.86	367.6	443	40.6	64.2
	12	6.39	11.44	179.05	357.6	419.1	38.2	58.5

Raw Table S2. Muscle wall thickness and Volume density of NF-M-positive fibers in the muscle layer of the rat stomach in control and STZ-NA group.

Group	Animal no	muscle wall thickness (μm)			NF-M Volume density of (%)		
		cardia	corpus	pylorus	cardia	corpus	pylorus
Control group	1	346.674	361.565	380.012	1.872	5.619	2.965
	2	371.388	397.79	416.37	4.304	2.998	3.869
	3	389.66	340.92	380.309	2.142	2.094	4.329
	4	328.105	359.435	411.07	3.978	3.896	5.003
	5	365.535	295.795	463.912	1.977	3.258	5.698
	6	440.704	335.747	426.315	3.997	4.5978	5.648
	7	374.429	371.07	430.571	5.705	4.239	3.986
	8	371.323	360.612	413.943	4.587	5.326	2.998
	9	381.306	335.128	402.135	3.986	4.003	3.269
	10	343.332	351.382	390.023	4.127	4.532	4.367
	11	338.263	401.832	379.141	4.866	2.896	5.514
	12	377.461	350.547	380.023	5.622	5.369	5.329

STZ-NA	1	373.712	342.77	410.802	3.617	5.624	5.326
	2	327.764	332.18	422.871	2.118	5.515	5.694
	3	365.16	393.325	386.67	5.123	1.977	2.069
	4	384.795	372.654	458.239	4.901	2.984	3.268
	5	398.278	362.789	418.05	3.993	3.258	4.318
	6	374.007	317.874	446.172	4.028	4.036	3.945
	7	346.025	393.994	417.793	2.979	5.359	4.085
	8	350.138	410.64	457.959	2.549	4.239	3.269
	9	313.844	390.928	413.636	3.712	4.396	2.896
	10	408.913	382.208	383.11	4.059	3.029	4.684
	11	359.279	297.895	382.265	5.601	2.986	4.239
	12	359.378	332.174	391.866	5.499	3.964	5.348

Raw Table S3. Volume density of NF-M positive fibers in the muscle layer of the rat stomach in control and STZ-NA group.

Group	Stomach region	N	X	SD	CV	Min	Max	ANOVA
			V_VNF					
Control	cardia	12	3.93	1.31	33.22	1.872	5.705	F=0.765
	corpus	12	4.07	1.10	27.03	2.094	5.619	P=0.682
	pylorus	12	4.41	1.02	23.13	2.965	5.698	
STZ-NA	cardia	12	4.01	1.12	27.90	2.118	5.601	F=0.149
	corpus	12	3.95	1.15	29.20	1.977	5.624	P=0.928
	pylorus	12	4.10	1.09	26.54		5.694	

N – specimen number, X – mean value, SD – standard deviation, CV – coefficient of variation

Raw Table S4. Numerical areal density (N_A) of intramuscular ICC of the circular (ICC-IMc) and longitudinal (ICC-IML) muscle layer of the rat stomach in control and STZ-NA group.

Stomach region		Group	N	X	SD	CV	Mann-Whitney
cardia	N_A ICC-IMc	control	106	198.45	46.25	23.31	Z=12.682
		STZ-NA	110	44.83	15.19	33.90	* P=0.000
	NA ICC-IML	control	106	23.11	12.21	52.80	Z=11.553
		STZ-NA	110	6.31	3.68	58.23	* P=0.000
corpus	N_A ICC-IMc	control	106	201.99	55.24	27.35	Z=12.280
		STZ-NA	105	49.97	28.88	57.78	* P=0.000
	N_A ICC-IML	control	106	24.34	10.78	44.28	Z=10.488
		STZ-NA	105	8.95	5.43	60.62	* P=0.000
pylorus	N_A ICC-IMc	control	102	100.31	28.52	28.43	Z=12.135
		STZ-NA	102	25.49	18.99	74.49	* P=0.000
	N_A ICC-IML	control	102	11.91	6.14	51.52	Z=4.408
		STZ-NA	102	8.37	4.72	56.38	* P=0.000

N – number of analyzed visual fields, X – mean value, SD – standard deviation, CV – coefficient of variation, N_{A-}numerical areal density – the average number of cells per mm^2 of the circular and longitudinal muscle layers.

Raw Table S5. Myenteric interstitial cells of Cajal (ICC-MP) score in the muscle layer of the rat stomach in control and STZ-NA group.

Stomach region	Group	N	X	SD	CV	Mann-Whitney
			MP-score (%)			
cardia	control	0				
	STZ-NA	0				
corpus	control	98	56.53	21.50	38.03	Z=9.708
	STZ-NA	98	20.71	15.68	75.71	*P=0.000
pylorus	control	107	54.39	16.95	31.15	Z=10.565
	STZ-NA	103	19.81	17.09	86.27	*P=0.000

N – total number of evaluated ganglions, X – mean value, SD – standard deviation, CV – coefficient of variation, * – statistical significance.